2.5D Finite Element Simulation – Eddy Current Heat Exchanger Tube Inspection using FEMM

Ashley L. PULLEN, Peter C. CHARLTON

Faculty of Applied Design and Engineering, University of Wales Trinity Saint David; Swansea, Wales, UK;
Phone: +44(0)1792 481000; e-mail: peter.charlton@uwtsd.ac.uk, ashley.pullen@outlook.com

Abstract

The paper describes the use of the open source electromagnetic finite element software package, FEMM used to simulate heat exchanger eddy current tube inspection. The paper provides an understanding of eddy current impedance plane responses to a number of defects using 2.5D axisymmetric finite element analysis. The scenarios examined are; corrosion, internal and external defects, baffle plate and baffle plate with fretting responses, internal defect, lift-off or improper fit and tube exit responses. A mathematical method of estimating the eddy current density as a function of penetration depth is also investigated with less than 5% over estimation. Finite element mesh optimisation is also investigated and a trade-off is made between accuracy and simulation time. Background knowledge on basic eddy current and heat exchangers is provided in the opening sections of the paper. Probe frequency variation and optimisation along with mesh boundaries are also discussed to help improve the simulation method. The effects of altering inspection frequency and the multiple effects this has on the inspection process are also discussed throughout the paper.

Keywords: Eddy Current, Tube Inspection, Finite Element Simulation, FEMM, Heat Exchanger Inspection, Eddy Current Skin Depth Penetration, Current Density, Mesh Optimisation, Phase Angle, Finite Element Analysis

1. Introduction

Eddy current inspection (ECT) has become the most widely used Non-Destructive Testing (NDT) methods for heat exchanger tube inspection. This paper discusses a finite element parametric study for a simulated heat exchanger inspection process using 100% IACS copper winding for the Eddy Current (EC) coil along with the heat exchanger. The study includes impedance plane diagrams to illustrate the effects that defect orientation and depth have on the eddy current coils phase angle and impedance.

Prior to the analyses process mesh optimisation is undertaken; this ensures an optimisation between result accuracy and computational time. Probe frequency optimisation is also considered.

The simulation of Eddy Current (EC) penetration depth and its relationship with frequency is analysed. A numerical approach in approximating the surface current density is also investigated with values extrapolated from the simulated results, coupled with the EC penetration depth formula where the Eddy Currents are 36.7% or 1/e of its surface value.

A simulation of insufficient probe fit is also investigated along with the effects of tube supports that are normally in place to enforce and support heat exchanger tubes. Multiple defect situations are also discussed and their impedance plane responses shown to aid in the understanding of EC impedance plane responses and the likely defect that is causing such a response.

2. Informative Literature

2.1 Eddy Current Probe

Eddy Current probes use the physics phenomenon of electromagnetic induction. In an EC probe an alternating current flows through a wire coil in turn generating an oscillating

magnetic field. If the probe and its magnetic field are brought near to a conductive material in this instance a heat exchanger tube, a circular flow of electrons also known as EC will begin to move through the metal perpendicular to the magnetic field as depicted below in Figure 1. The EC flowing through the material will generate its own magnetic field that will interact with the coil and its field through mutual inductance. The presence of a defect or a change in wall thickness will result in the alteration of the amplitude and pattern of the EC and its resultant magnetic field. This alteration has a direct effect on the EC coil by altering its electrical impedance as seen in Figure 1. This change in impedance value and phase angle is then recorded and displayed by the EC instrumentation for the interpretation of the operator.

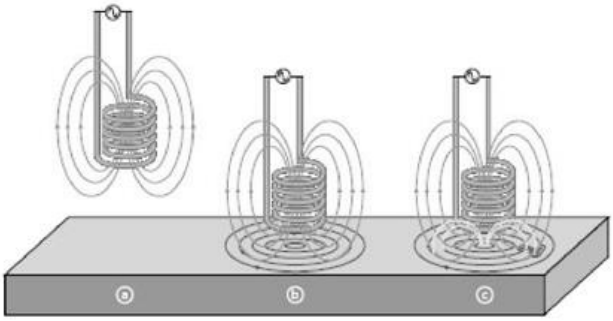

Figure 1: Showing induced EC and its effects [1]

EC density is at its highest at the surface of the inspection specimen resulting in the region of highest resolution. The standard depth of penetration is defined as the depth at which the current density is 1/e of its surface value, this phenomenon is known as the 'Skin Effect' and may be calculated using the following formula;

$$\delta_{mm} = \frac{661}{\sqrt{f \mu_r \sigma}} \tag{1}$$

Where; δ = Standard depth of penetration (mm)
f = Test frequency (Hz)
μ_r = Relative Permeability (dimensionless, = 1 for non-ferrous materials)
σ = Electrical Conductivity (%IACS)

From the above formula it is possible to see that the depth to which EC's penetrate into a material is directly related to the excitation frequency, the electrical conductivity, and the magnetic permeability of the specimen. It is also possible to indicate that the depth of penetration decreases with higher frequency levels, increasing magnetic permeability, and conductivity.

Prior to an EC inspection a frequency should be selected in order to penetrate to the back wall in situations of lesser wall thicknesses, or at a depth where defects are expected. Doing so allows for sufficient current density to ensure the necessary flaw detection.

2.2 Heat Exchangers

Shell and tube heat exchangers are one of the most widely used type of heat exchangers in the processing industries and are commonly found in oil refineries, nuclear power plants, and other large-scale chemical processes. There are a number of possible configurations for heat

exchangers, but their basic concept can be shown with the description of some key components. An example of a typical shell and tube heat exchanger is shown in Figure 2.

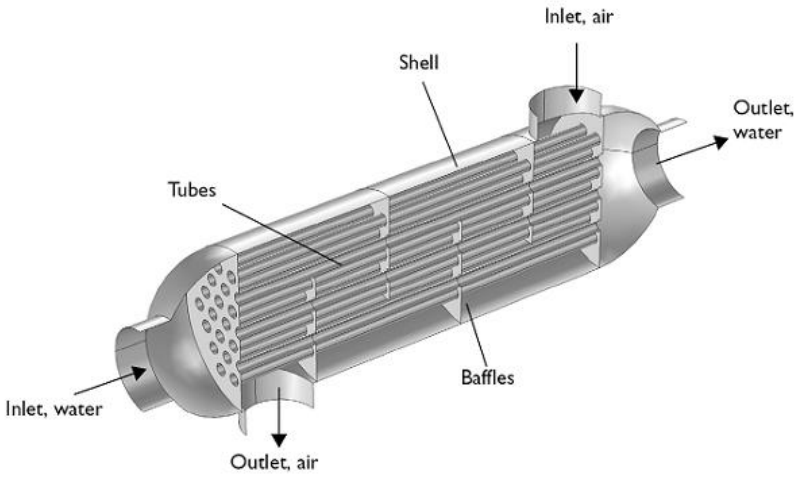

Figure 2: Showing a typical shell and tube type heat exchanger [2]

From Figure 2 it is possible to see that heat exchangers operate by transferring heat from one median to another. From the above example 'Hot Air' would enter through the 'Air Inlet' that then flows through the heat exchanger in a rotational manner. This rotational flow of the air is forced by the heat exchangers cylindrical geometry and its baffle plates. This allows for circulation through the full heat exchanger increasing the path length resulting in increased levels of heat transfer. Water is pumped to the 'Water Inlet Tubes' through the heat exchanger allowing heat transfer between the 'Hot Air' and the 'Water' to take place.

Due to the moisture levels within the heat exchanger caused from both the internal flowing water and the condensing air on the outer diameter of the tubes, it is clear that the oxidisation of the tubes is inevitable resulting in wall ruptures and leaking tubes. This can cause major disruptions in chemical plants forcing decommission until this problem is rectified.

2.3 Eddy current examination method

This method employs a probe (bobbin type) that contains one or more alternating current (AC) coils that induce an electric field in the tube as previously stated in section 2.1. Prior to the inspection process it is necessary that the EC system has been calibrated on a reference standard with known, machined discontinuities, an example of this may be seen in Figure 3. The probe is usually fired down the inspection tube and drawn back using an electric motor machine at a constant speed; changes in coil impedance are recorded. The data may then be displayed on a screen for data analysis and evaluation. Phase analysis and signal amplitude are utilised to assess the depth, origin and size of flaws [3].

2.3.1 Advantages

- Inspection speed up to approximately 60 feet per minute
- Can detect gradual wall thinning and localised flaws
- Provides both phase and amplitude information
- Permanent records can be obtained on test results
- By using multi-frequency techniques, flaws under the support plates (baffles) can be found and evaluated accurately

2.3.2 Limitations

- Limited to only non-magnetic tube material
- Requires high inspection skills for data analysis and evaluation
- Tubes must be cleaned
- Discontinuities adjacent to end sheets are difficult to detect

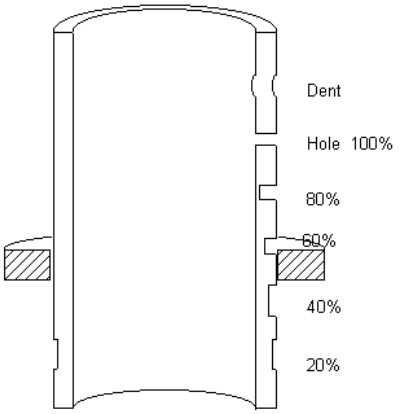

Figure 3: Showing ASME Calibration Tube with Support Plate [4].

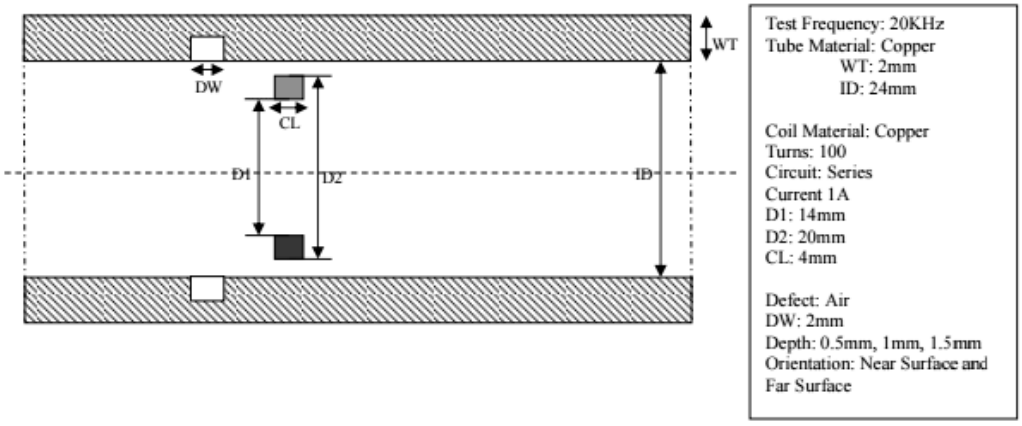

Figure 4: Showing EC inspection Model

3. EC Model

Figure 4 shows the parameters used for modelling of the 2.5D axisymmetric inspection simulation. The copper used in this inspection simulation is 100%IACS for both the coil and tube material as previously stated.

3.1 Mesh Optimisation

Mesh optimisation is a process that will allow for the comparison of mesh density and the accuracy of results produced by 'Finite Element Analysis' software. For this process an area of interest is to be investigated and an extractable result value should be available for data processing in the form of tables and then converted into a graphical representation. This allows for the optimal point to be selected between mesh size and computational time. The results of this process are shown below in Table 1 & Figure 5. As can be seen in Figure 5 after a mesh density of 0.05 is reached the results do not increase at a significant rate, taking this into consideration accompanied by an acceptable computational time a mesh size of 0.05 is chosen.

Within the FEMM software package the mesh size does not directly correspond to a mesh area, although this may be calculated by extrapolating the vector co-ordinates and solving the area. This process of vector summation to calculate the Mesh Area was undertaken with the results displayed in Table 2.

Table 1: Showing Mesh Density results

Mesh Density	Magnetic Energy
1	4.03E-11
0.5	4.06E-11
0.3	4.07E-11
0.2	4.08E-11
0.1	4.10E-11
0.05	4.10E-11
0.025	4.11E-11
0.01	4.11E-11

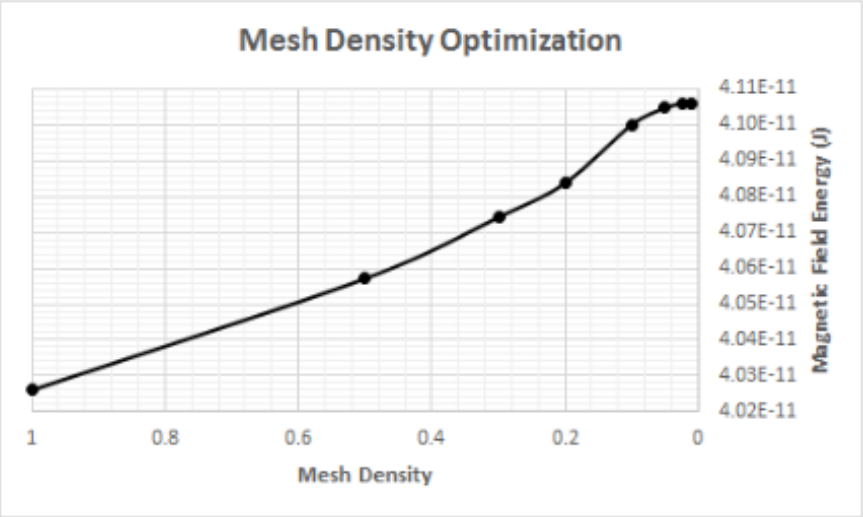

Figure 5: Showing mesh density optimisation plot

Table 2: Showing Mesh Density with the Mesh Area.

Mesh Density	Mesh Area (mm^2)
1	0.717
0.05	0.01

3.2 Mesh Boundaries

In order to further improve computational time mesh boundaries have been set. This allows for increased mesh densities within areas of interest and a lesser density where it is not so important. The mesh boundaries set can be seen in Figure 6.

The positioning of these boundaries ensures the best results from simulation process maintaining an even distance from the centre of the defect. The defect is positioned central to the tube to minimise the 'Edge Effect' from either ends of the modelled tube.

3.3 Probe Optimisation

It is possible to calculate the optimal frequency at which to set an EC probe when undergoing an inspection process. This is done by the manipulation of the 'Skin Depth' formula previously discussed (See formula 1). The resultant rearrangement is as follows;

$$f = \frac{1}{\mu_r \sigma}\left(\frac{661}{\delta}\right)^2 \quad (2)$$

Applying this formula with the value δ, equal to the wall thickness (mm), μ_r to be 1 and σ to 100%IACS. The optimum probe frequency is 1092.3025 Hz. This is where the 1/e penetration depth is equivalent to the wall thickness. Lowering the frequency has an adverse effect on the detection resolution but increasing the detection sensitivity, this will be discussed further in the analysis section.

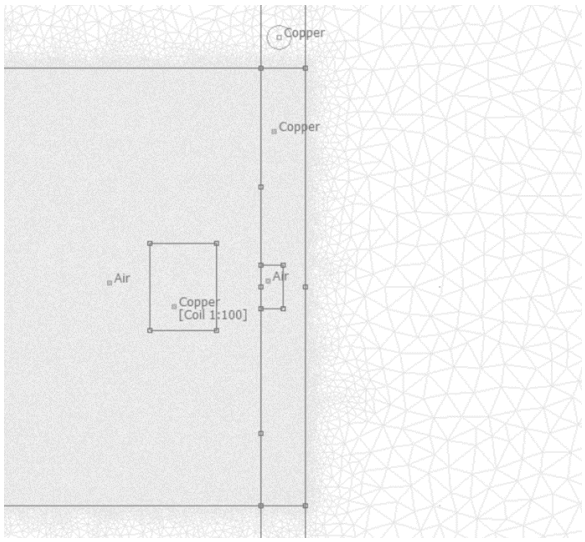

Figure 6: Showing mesh boundaries and optimisation density

4. Results & Analysis

4.1 Calculating the Circuit Impedance

The circuit Impedance (Z) is the total opposition that a circuit presents to alternating current. Impedance is measured in Ohms and is calculated using Resistance (R) and Inductive Reactance (X_L). Vector summation is used in order to calculate the impedance value. The required formula may be seen as follows in equation (3);

$$Impedance = \sqrt{R^2 + X_L^2} \tag{3}$$

Where; R = Resistance, and X_L = Inductive Reactance.

4.2 Impedance Plane Balancing

It is possible to balance the impedance plane as would be done on an EC set. This is done by simulating a defect free scenario. The resistance and inductive reactance values are then recorded in order to subtract from the simulated defect results.

The results for internal defects are shown in Figures 7, 8, and 9.

4.3 Calculating the Phase Angle

The phase angle is calculated from the R and X_L values obtained from the simulation results. The phase angle θ is calculated as shown in equation (4);

$$Phase\ Angle\ (\theta) = \tan^{-1}\frac{X_L}{R} \tag{4}$$

Where; R = Resistance, and X_L = Inductive Reactance.

4.4 Depth of EC Penetration

It is possible to calculate the standard depth of penetration of the EC set-up from equation (1). As previously discussed the depth of penetration is directly inversely proportional to the frequency of the EC probe, permeability, and the electrical conductivity of the specimen.

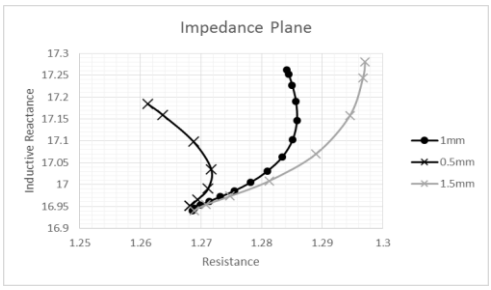

Figure 7: Showing Impedance plane response of internal defects

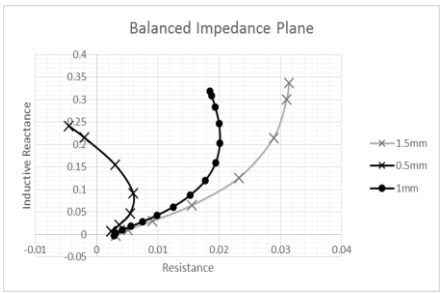

Figure 8: Balanced impedance plane response signal

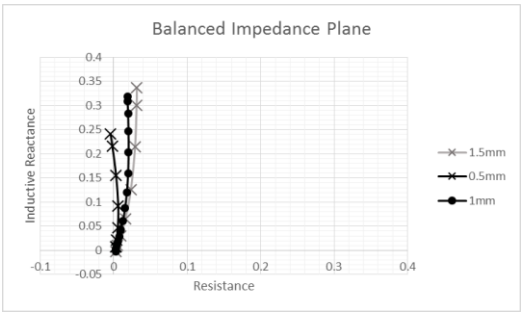

Figure 9: Phase angle representation from equal axis

4.5 Numerical Estimation of EC Surface Density

The computational methods used in FEMM for current density are not capable of calculating the current density directly at the surface of the specimen, as shown in Figure 10.

A form of estimating the surface current density is undertaken based on the standard depth of penetration formula (1) and the current density results obtained from FEMM.

Firstly one standard depth of penetration is calculated, for the results shown in Figure 10 for 10 KHz probe. Therefore it is known that at one standard depth of penetration the current density is 1/e of the value at the surface. Therefore it is possible to estimate this surface current density using equation (5);

$$Surface\ Current\ Density = \frac{CD_{\delta}}{1 \div e} \tag{5}$$

Where; CD_{δ} = current density at one standard depth of penetration.

Equation (5) gives a value for the EC density at the internal surface of the tube; from this the formula of exponential decay is applied to numerically estimate the current decay as a function of penetration distance. In order to do this, first the exponential decay coefficient is required to be calculated from the exponential decay equation (6);

$$J_0\, e^{-\alpha\, \delta} = J_x \tag{6}$$

$$e^{-\alpha\,\delta} = \frac{J_0}{J_x} \tag{7}$$

$$e^{-\alpha\,\delta} = \frac{1}{e} \tag{8}$$

$$\alpha = -\frac{ln\left(\frac{1}{e}\right)}{\delta} \tag{9}$$

Where; J_0 = Surface current density, J_x = the current density at one standard depth of penetration, δ = one standard depth of penetration, α = the decay coefficient.
From equation (9) the decay coefficient may be calculated for a specific problem where δ, J_0, and J_x have been calculated. Knowing this it is possible to apply the resultant value of the exponential decay formula (10);

$$J_0\, e^{-\alpha\,\delta} = CD \tag{10}$$

Where; J_0 = the surface current density, x = the distance to the point of required density, CD = newly calculated current density, and α = as calculated from equation (9).

Apply equation (10) to the same range of penetration depths as used by the FEMM simulation model. With the following (Figure 11);

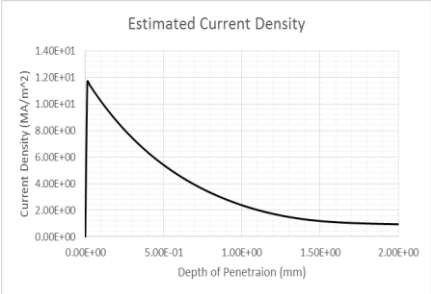

Figure 10: Showing current density calculated by FEMM for a 10 KHz probe

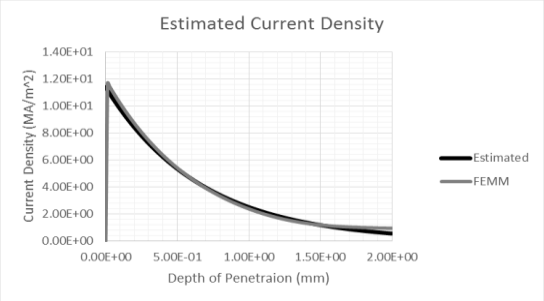

Figure 11: Showing numerically estimated and FEMM calculated current density

4.6 Phase Lag

The phase lag is a parameter of the eddy current system that makes it possible to determine the depth of a defect. Phase lag is the shift in time between the eddy current response from a disruption of the surface and below. Disruption or flaws in the material cause a higher phase lag at increased depths. Due to the phase lag disruption of a deeper defect a clear difference is seen on the test plane impedance vector. The phase lag may be calculated using the following equation (11);

$$Phase\ Lag = \frac{x}{\delta} \times 57.3 \tag{11}$$

Therefore by measuring the phase lag of a signal the defect depth may be estimated.

$$\theta . \frac{\delta}{57.3} = x \tag{12}$$

Where; θ = phase angle, δ = one standard depth of penetration, and x = defect depth.

4.7 Defect Depth and Impedance Change

Based upon equation (3) for the impedance value the relationship between impedance values and defect depth is produced, figure 12.

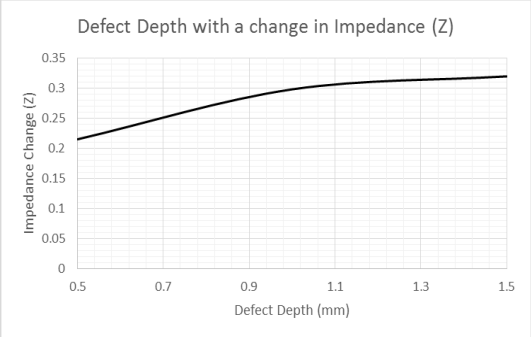

Figure 12: Showing the relationship between defect depth and the impedance values

From figure 12 it is possible to see that when the defect depth increases an impedance change results. As the depth increases there is less change in the impedance value. This is due to the penetration depth of the 20 kHz probe frequency used.

4.8 Back Wall Defect Response

This section will look at the results obtained from outer defect responses at 20 kHz and an optimal frequency of 1092Hz, as determined using the depth of penetration equation (2). A depth of penetration curve for the tube material is given in figure 13. The results show that the decrease in frequency will result in an increase in the response to smaller external defects due to the increased current penetration at lower frequencies.

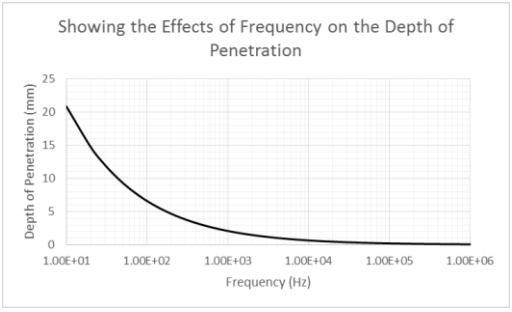

Figure 13: Showing the depth of penetration as a function of frequency

4.8.1 20 kHz Impedance Plane Response

The largest defect size of 1.5mm is detected at this frequency whereas the 1mm and 0.5mm defects are not detected or show a minimal response resulting in an unclear indication. See Figure 14.

4.8.2 Optimal Frequency Impedance Plane Response

From figure 15, the impedance plane signal response using the optimal probe frequency shows that all defects are clearly indicated as expected. The change in frequency results in a more significant visual change in impedance values with defect depth as seen in Figure 16.

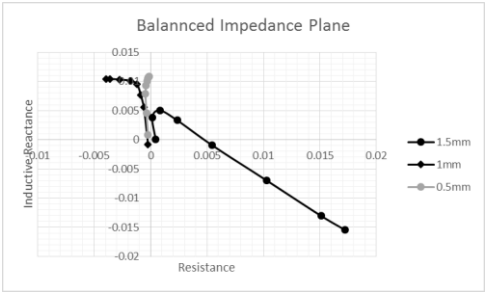

Figure 14: Showing the balanced impedance plane for outer wall defects with a 20 KHz frequency

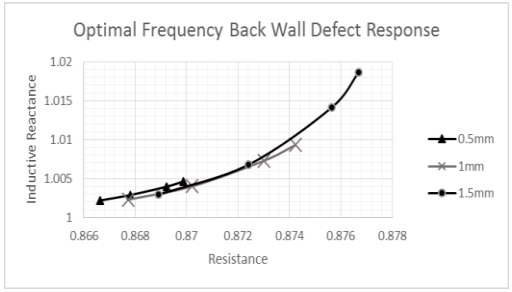

Figure 15: Showing optimal frequency impedance plane response to outer wall defects

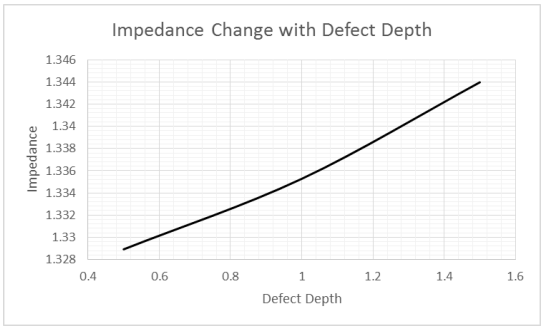

Figure 16: Showing the impedance response as a function of defect depth

4.9 Baffle Plate and Fretting Impedance Plane Signal Responses

Baffle plates are a component within heat exchangers that both support the heat exchanger tubes and aid air flow. Due to the position of the baffle plates it is possible that the eddy current inspection procedure will be affected by these components and in particular at lower eddy current frequencies.

Two simulations have been undertaken to mimic the signal responses of the impedance plane vector in order to pre-determine what is seen if a baffle plate or a baffle plate with fretting is encountered during an inspection procedure.

Fretting refers to wear or corrosion of two surfaces that are in contact, and is caused by repeated motion under load.

A typical meshed model is given in figure 17. The results obtained from the simulated inspection over baffle plates with and without fretting are seen below in Figure 18.

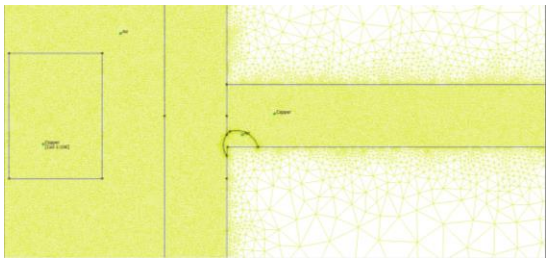

Figure 17: Showing FEMM model for baffles with fretting. The same model is used for with the alteration of the material properties of the fretting region to copper.

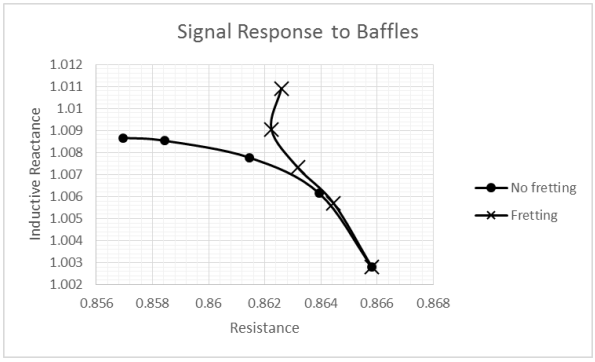

Figure 18: Showing impedance response to a baffle with and without fretting

As can be seen from the above figure if balancing was to occur all results would be shown in the negative quadrant. It can be seen that a baffle plate produces a smooth curve with lesser resistance when nearing the baffle plate with increased levels of Inductive Resistance.

When a baffle plate with fretting is inspected it is clear to see that there are increased levels of resistance at the same probe positions when compared to a defect free baffle plate. A significant rise in Inductive Reactance is also seen when the probe is central to the defected baffle plate.

4.10 Internal Wall Defect Response

This section will show the simulated results of the impedance plane with respect to an internal defect of 0.5mm at a depth of 0.5mm below the surface. The signal response expected is not similar to what has already been seen due to the nature of the internal defect as the current flow around it will affect the results. A typical mesh and resulting impedance plane may be seen in Figures 19 and 20.

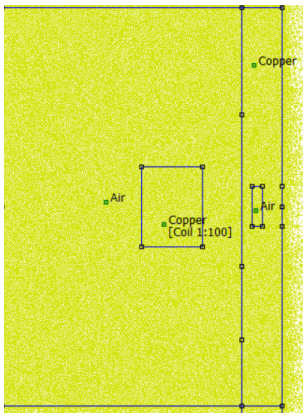

Figure 19: Internal defect

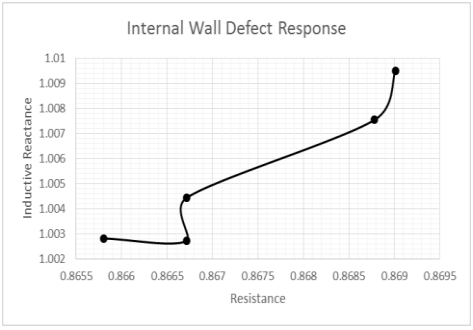

Figure 20: Showing the impedance plane response for an internal defect.

4.11 Complex Internal Surface Response

A complex response is seen to occur due to a complex internal surface profile. The initial drop in inductive reactance is due to a wall thickness increase, when the surface thickness decreases a rise in inductive reactance is seen. A typical model and impedance plane response is given in figures 21 and 22.

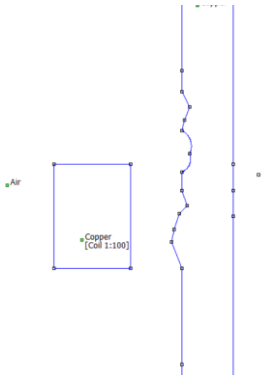

Figure 21: Complex/Corroded internal surface

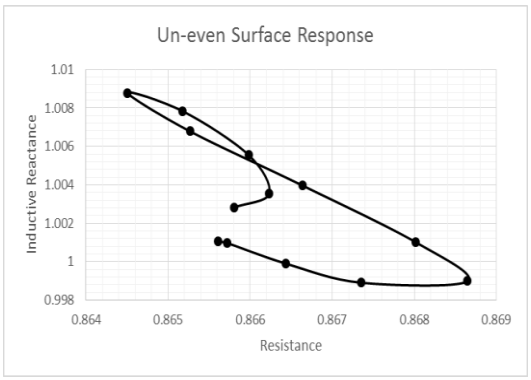

Figure 22: Showing a typical impedance plane scan of an Un-even surface

4.12 Improper Fit Response

Figure 23 shows the results of proper and improper fit of a 20 KHz probe with a response comparison of a 1mm surface defect. The improper fit has an extra clearance of 1.5mm to the tube wall. This result is a lower sensitivity meaning that defects could be missed.

4.13 Tube Exit

Figure 24 indicates the expected impedance plane when exiting the inspection tube, a vast increase in Inductive Reactance is seen when the probe leaves the tube.

Figure 23: Proper and improper fit for a 1mm defect at 20 KHz

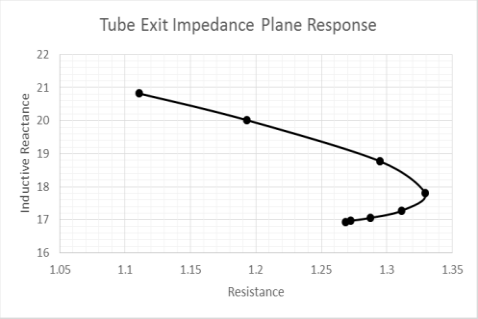

Figure 24: Tube exit impedance plane response

4.14 Phase Lag and Angle Change

The Phase angle change of an EC set-up is dependent upon the inspection frequency used. This section will graphically represent the changes of phase angle and also the phase lag that is expected at various depths from the inspection frequency used. It is expected that the lower the inspection frequency the lesser the phase angle change and also the phase lag at a particular depth [5].

4.14.1 Inspection Frequency: 20 kHz

For an inspection frequency of 20 kHz a high degree of phase change is expected. The results of the overall phase change can be seen in Figure 25. The total change in phase angle is then shown in Figure 26 and compared with the phase lag indicating a similar trend with almost identical values showing a relationship between the two.

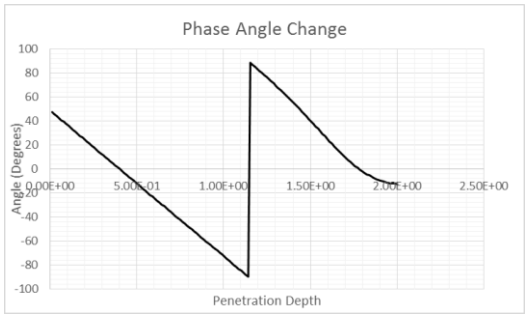

Figure 25: Phase Change of a 20 KHz inspection frequency

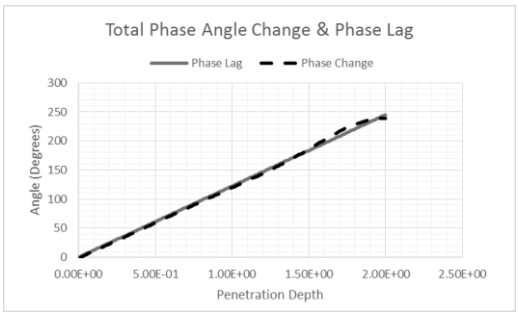

Figure 26: Showing total phase change and phase lag as a function of penetration depth (mm)

4.14.2 Inspection Frequency: 10 kHz

Lowering of the inspection frequency alters the change in phase angle and phase lag. As can be seen in Figure 27 the phase angle change is less than that of the 20 kHz frequency. The total phase angle change and phase lag as a function of penetration depth is almost 100 degrees less than that of the 20 kHz inspection frequency.

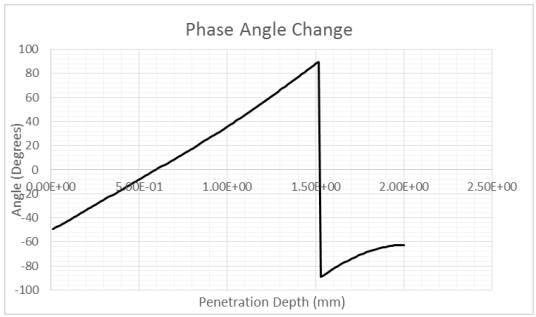

Figure 27: Phase angle change as a function of penetration depth

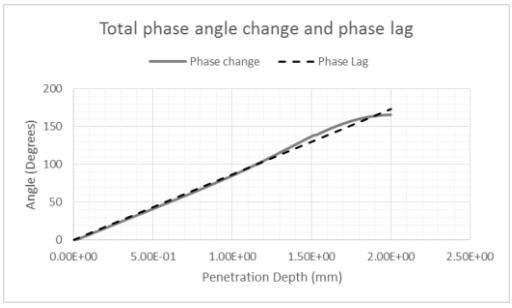

Figure 28: showing phase lag and total phase angle change relationship

4.14.3 Inspection Frequency: Optimal (1092.303 Hz)

The phase change is shown below in Figure 29, along with the phase lag. The phase lag and total phase change has further reduced, although there is not a significant relationship between the two after 1mm depth of penetration.

4.15 Phase angle as a function of defect depth

As previously stated the phase angle can be used to estimate the depth of a defect. The corresponding phase as a function of defect depth is seen below in Figure 30.

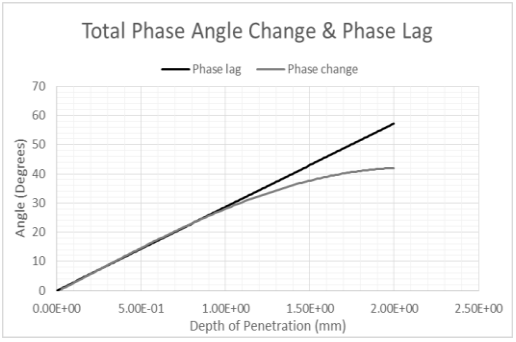

Figure 29: Showing phase lag and total phase angle change as a function of penetration depth

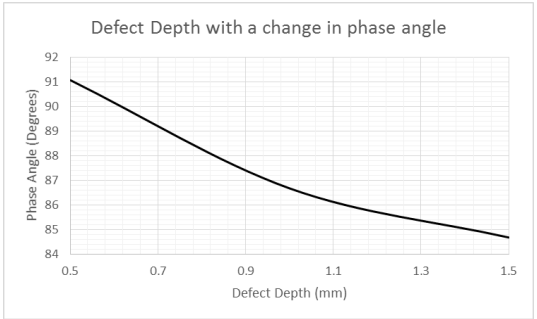

Figure 30: Showing the phase angle change of a defect depth of a surface defect

5. Conclusion

Multiple defect types and associated EC impedance plane responses have been estimated using finite element analysis. The most common types of encounters of an EC tube/heat exchanger inspection have been investigated. This provides an overview of what to expect during an inspection and what is likely to be causing the impedance plane shown.

Altering the frequency of an EC probe has a direct effect on both the depth of penetration and the sensitivity of the process.

The higher the test frequency the higher the resolution but a lower sensitivity to defects is seen. A lower frequency is resultant in an increased sensitivity due to the penetration depth of the EC's with a lower resolution.

Numerically calculated current density is considerably accurate with the estimated values on average being 104.66% of the FEMM results. Meaning an over estimation of 4.66%. This oversizing is most significantly seen in the later quadrant between 1.5 and 2mm penetration depths.

Improper fit where excessive lift off occurs is resultant in a lower detection sensitivity meaning it is possible to miss small discontinuities, and would not achieve full penetration for outer wall defects.

Overall it has been shown that the FEMM software package is more than capable of providing eddy current tube inspection optimisation.

Acknowledgements

The authors would like to acknowledge the financial support of the Access to Masters (ATM) scheme.

References

1. Nelligan, Tom and Calderwood, Cynthia. Introduction to Eddy Current Testing. *Olympus.* [Online] 2015. [Cited: 24 04 2015.] http://www.olympus-ims.com/en/eddycurrenttesting/.

2. Foley, Alexandra. How to Model a Shell and Tube Heat Exchanger. *comsol.* [Online] 11 September 2013. [Cited: 24 April 2015.] http://www.comsol.com/blogs/how-model-shell-and-tube-heat-exchanger/

3. Sadek, H. *NDE technologies for the examination of heat exchangers and boiler tubes - principles, advantages and limitations.* Charlotte, NC [USA] : NDT.NET, 2006.

4. O'Connor, Monty. Eddy Current Testing of Heat Exchanger Tubes Is Not Quite That Easy. *eddy-current.com.* [Online] Eddy Current Technology, Inc., October 2013. [Cited: 24 April 2015.] http://eddy-current.com/eddy-current-testing-of-heat-exchanger-tubes-is-not-quite-that-easy/

5. Phase Lag. *NDT.* [Online] NDT Resource Centre. [Cited: 03 05 2015.] www.nde-ed.org/EducationResources/CommunityCollege/EddyCurrents/Physics/phaselag.htm.